



Supplement of

Oligomer formation from the gas-phase reactions of Criegee intermediates with hydroperoxide esters: mechanism and kinetics

Long Chen et al.

Correspondence to: Yu Huang (huangyu@ieecas.cn)

The copyright of individual parts of the supplement might differ from the article licence.

Contents:

Table S1 The electronic energy (ΔE^\ddagger) and Gibbs free energy (ΔG^\ddagger) barriers for the initial reactions of distinct SCIs with HCOOH predicted at the Y/X (Y = M06-2X, CCSD(T) and QCISD(T), X = ma-TZVP, 6-311+G(2df,2p) level based on the M06-2X/6-311+G(2df,2p) optimized geometries (kcal mol⁻¹)

Table S2 Enthalpies of formation ($\Delta_f H_{298}^\circ$) for the various carbonyl oxides and hydroperoxide esters computed at the CCSD(T)//M06-2X/6-311+G(2df,2p) level of theory

Table S3 Rate coefficients (cm³ molecule⁻¹ s⁻¹) of each elementary pathway involved in the initiation reaction of CH₂OO with HCOOH computed at different temperatures

Table S4 Rate coefficients (cm³ molecule⁻¹ s⁻¹) of each elementary pathway involved in the initiation reaction of *anti*-CH₃CHOO with HCOOH computed at different temperatures

Table S5 Rate coefficients (cm³ molecule⁻¹ s⁻¹) of each elementary pathway involved in the initiation reaction of *syn*-CH₃CHOO with HCOOH computed at different temperatures

Table S6 Rate coefficients (cm³ molecule⁻¹ s⁻¹) of each elementary pathway involved in the initiation reaction of (CH₃)₂OO with HCOOH computed at different temperatures

Table S7 Rate coefficients of distinct SCIs reactions with Pent1a computed at different temperatures

Table S8 Predicted saturated vapour pressure (P⁰) and saturated concentrations (c⁰) for the adduct products of the successive reactions of SCIs with HCOOH

Figure S1. The geometries of all the stationary points for distinct SCIs reactions with formic acid optimized at the M06-2X/6-311+G(2df,2p) level of theory

Figure S2. Electronic potential energy along the O-H and C-O distance (angstroms) calculated by the M06-2X/6-311+G(2df,2p) method for the 1,4-insertion reactions CH₂OO + HCOOH (a), *anti*-CH₃CHOO + HCOOH (b), *syn*-CH₃CHOO + HCOOH (c) and (CH₃)₂COO + HCOOH (d) (the black solid line represents the minimum potential-energy path (MEP))

Figure S3. The geometries of all the stationary points for 2CH₂OO + Pent1a reaction optimized at the M06-2X/6-311+G(2df,2p) level of theory

Figure S4. Natural bond orbital (NBO) analysis of the donor-acceptor orbitals involved in the TS1a

Figure S5. The geometries of all the stationary points for 2*anti*-CH₃CHOO + Pent1b reaction optimized at the M06-2X/6-311+G(2df,2p) level of theory

Figure S6. The geometries of all the stationary points for 2*syn*-CH₃CHOO + Pent1c reaction optimized at the M06-2X/6-311+G(2df,2p) level of theory

Figure S7. The geometries of all the stationary points for 2(CH₃)₂COO + Pent1d reaction optimized at the M06-2X/6-311+G(2df,2p) level of theory

Figure S8. The geometries of all the stationary points for distinct SCIs reactions with Pent1a optimized at the M06-2X/6-311+G(2df,2p) level of theory

Figure S9 The NPA charges of different atoms in the distinct SCIs computed at the M06-2X/6-311+g(2df,2p) level of theory

Figure S10. The optimized geometries and relative energies (kcal·mol⁻¹) computed for the four conformers of MVK-oxide. Geometries are optimized at the M06-2X/6-311+g(2df,2p) level of theory. Single point energies are calculated at the CCSD(T)/6-311+g(2df,2p) level of theory

Table S1 The electronic energy (ΔE^\ddagger) and Gibbs free energy (ΔG^\ddagger) barriers for the initiation reactions of distinct SCIs with HCOOH predicted at the Y/X (Y = M06-2X, CCSD(T) and QCISD(T), X = ma-TZVP, 6-311+G(2df,2p) level based on the M06-2X/6-311+G(2df,2p) optimized geometries (kcal mol⁻¹)

	M06-2X/ ma-TZVP		CCSD(T)/ 6-311+G(2df,2p)		QCISD(T)/ 6-311+G(2df,2p)	
	ΔE^\ddagger	ΔG^\ddagger	ΔE^\ddagger	ΔG^\ddagger	ΔE^\ddagger	ΔG^\ddagger
	Entry 2					
CH ₂ OO	8.0	10.0	8.6	10.5	8.7	10.7
<i>anti</i> -CH ₃ CHOO	12.0	13.0	11.0	11.9	10.9	12.0
<i>syn</i> -CH ₃ CHOO	13.1	14.6	13.3	14.9	13.2	14.8
Entry 3						
CH ₂ OO	20.6	21.8	20.4	21.6	20.6	21.8
<i>anti</i> -CH ₃ CHOO	20.6	22.2	20.2	21.8	20.2	21.8
<i>syn</i> -CH ₃ CHOO	25.7	27.6	25.6	27.7	25.8	27.7
Entry 4						
CH ₂ OO	4.4	5.8	4.2	5.6	4.3	5.7
<i>anti</i> -CH ₃ CHOO	4.1	5.6	3.3	4.9	3.4	4.9
<i>syn</i> -CH ₃ CHOO	8.9	11.1	8.5	10.9	8.6	10.8

Table S2 Enthalpies of formation ($\Delta_f H_{298}^{\circ}$) for the various carbonyl oxides and hydroperoxide esters computed at the CCSD(T)//M06-2X/6-311+G(2df,2p) level of theory

Species	Cal (kcal·mol ⁻¹)	Refs. (kcal·mol ⁻¹)
CH ₂ OO	23.23	22.92 ^a 24.59 ^b
<i>anti</i> -CH ₃ OO	10.28	
<i>syn</i> -CH ₃ CHOO	6.73	
(CH ₃) ₂ COO	-6.77	
HCOOH		-90.62 (exp)
HC(O)OCH ₂ OOH (Pent1a)	-112.08	
HC(O)OCH(CH ₃)OOH (Pent1b)	-124.20	
HC(O)OCH(CH ₃)OOH (Pent1c)	-122.02	
HC(O)OC(CH ₃) ₂ OOH (Pent1d)	-134.51	

Exp is taken from NIST Chemistry Webbook

^a the value is obtained at the G4 level of theory (Chen et al., 2016)

^b the value is obtained at the W3-F12 level of theory (Karton et al., 2013)

Chen, L., Wang, W., Wang, W., Liu, Y., Liu, F., Liu, N., and Wang, B: Water-catalyzed decomposition of the simplest Criegee intermediate CH₂OO, *Theor. Chem. Acc.*, 135, 131-143, <https://doi.org/10.1007/s00214-016-1894-9>, 2016.

Karton, A., Kettner, M., and Wild, D. A.: Sneaking up on the Criegee intermediate from below: Predicted photoelectron spectrum of the CH₂OO⁻ anion and W3-F12 electron affinity of CH₂OO, *Chem. Phys. Lett.*, 585, 15-20, <http://doi.org/10.1016/j.cplett.2013.08.075>, 2013.

Table S3 Rate coefficients ($\text{cm}^3 \text{ molecule}^{-1} \text{ s}^{-1}$) of each elementary pathway involved in the initiation reaction of CH_2OO with HCOOH computed at different temperatures

T/K	$k(\text{TS}_{\text{ent}1})$	$k(\text{TS}_{\text{ent}2})$	$k(\text{TS}_{\text{ent}3})$	$k(\text{TS}_{\text{ent}4})$	$k_{\text{tot-CH}_2\text{OO}}$
273	1.34×10^{-10}	3.56×10^{-12}	1.03×10^{-22}	3.57×10^{-12}	1.41×10^{-10}
280	1.30×10^{-10}	2.94×10^{-12}	1.22×10^{-22}	3.12×10^{-12}	1.36×10^{-10}
298	1.25×10^{-10}	1.88×10^{-12}	2.18×10^{-22}	2.26×10^{-12}	1.29×10^{-10}
300	1.21×10^{-10}	1.80×10^{-12}	2.35×10^{-22}	2.20×10^{-12}	1.25×10^{-10}
320	1.17×10^{-10}	1.18×10^{-12}	4.86×10^{-22}	1.63×10^{-12}	1.20×10^{-10}
340	1.12×10^{-10}	8.16×10^{-13}	1.04×10^{-21}	1.26×10^{-12}	1.14×10^{-10}
360	1.11×10^{-10}	5.92×10^{-13}	2.20×10^{-21}	1.04×10^{-12}	1.13×10^{-10}
380	1.07×10^{-10}	4.48×10^{-13}	4.52×10^{-21}	8.23×10^{-13}	1.08×10^{-10}
400	1.05×10^{-10}	3.50×10^{-13}	9.01×10^{-21}	6.91×10^{-13}	1.06×10^{-10}

Table S4 Rate coefficients ($\text{cm}^3 \text{ molecule}^{-1} \text{ s}^{-1}$) of each elementary pathway involved in the initiation reaction of *anti*- CH_3CHOO with HCOOH computed at different temperatures

T/K	$k(\text{TS}_{\text{ent1-anti}})$	$k(\text{TS}_{\text{ent2-anti}})$	$k(\text{TS}_{\text{ent3-anti}})$	$k(\text{TS}_{\text{ent4-anti}})$	$k_{\text{tot-anti}}$
273	4.94×10^{-10}	4.23×10^{-11}	5.53×10^{-22}	6.12×10^{-11}	5.98×10^{-10}
280	4.82×10^{-10}	3.75×10^{-11}	6.73×10^{-22}	4.92×10^{-11}	5.69×10^{-10}
298	4.69×10^{-10}	2.34×10^{-11}	1.20×10^{-21}	2.95×10^{-11}	5.22×10^{-10}
300	4.56×10^{-10}	2.01×10^{-11}	1.29×10^{-21}	2.80×10^{-11}	5.04×10^{-10}
320	4.42×10^{-10}	1.48×10^{-11}	2.61×10^{-21}	1.72×10^{-11}	4.74×10^{-10}
340	4.28×10^{-10}	9.42×10^{-12}	5.36×10^{-21}	1.12×10^{-11}	4.49×10^{-10}
360	4.27×10^{-10}	7.04×10^{-12}	1.08×10^{-20}	7.77×10^{-12}	4.42×10^{-10}
380	4.14×10^{-10}	3.64×10^{-12}	2.12×10^{-20}	5.60×10^{-12}	4.23×10^{-10}
400	4.09×10^{-10}	2.02×10^{-12}	4.01×10^{-20}	4.18×10^{-12}	4.15×10^{-10}

Table S5 Rate coefficients ($\text{cm}^3 \text{ molecule}^{-1} \text{ s}^{-1}$) of each elementary pathway involved in the initiation reaction of *syn*- CH_3CHOO with HCOOH computed at different temperatures

T/K	$k(\text{TS}_{\text{ent1-syn}})$	$k(\text{TS}_{\text{ent2-syn}})$	$k(\text{TS}_{\text{ent3-syn}})$	$k(\text{TS}_{\text{ent4-syn}})$	$k_{\text{tot-syn}}$
273	2.34×10^{-10}	9.50×10^{-13}	4.58×10^{-27}	7.46×10^{-16}	2.35×10^{-10}
280	2.25×10^{-10}	8.03×10^{-13}	7.06×10^{-27}	6.43×10^{-16}	2.26×10^{-10}
298	2.17×10^{-10}	5.37×10^{-13}	8.92×10^{-26}	5.46×10^{-16}	2.18×10^{-10}
300	2.08×10^{-10}	5.15×10^{-13}	9.94×10^{-26}	4.58×10^{-16}	2.09×10^{-10}
320	1.99×10^{-10}	3.55×10^{-13}	3.03×10^{-25}	3.78×10^{-16}	1.99×10^{-10}
340	1.89×10^{-10}	2.57×10^{-13}	9.14×10^{-25}	3.05×10^{-16}	1.89×10^{-10}
360	1.88×10^{-10}	1.95×10^{-13}	2.64×10^{-24}	3.03×10^{-16}	1.88×10^{-10}
380	1.79×10^{-10}	1.53×10^{-13}	7.15×10^{-24}	2.43×10^{-16}	1.79×10^{-10}
400	1.76×10^{-10}	1.24×10^{-13}	1.82×10^{-23}	2.22×10^{-16}	1.76×10^{-10}

Table S6 Rate coefficients ($\text{cm}^3 \text{ molecule}^{-1} \text{ s}^{-1}$) of each elementary pathway involved in the initiation reaction of $(\text{CH}_3)_2\text{OO}$ with HCOOH computed at different temperatures

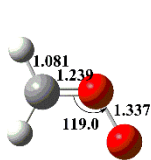
T/K	$k(\text{TS}_{\text{ent1-dim}})$	$k(\text{TS}_{\text{ent2-dim}})$	$k(\text{TS}_{\text{ent3-dim}})$	$k(\text{TS}_{\text{ent4-dim}})$	$k_{\text{tot-dim}}$
273	4.10×10^{-10}	6.81×10^{-12}	1.38×10^{-26}	4.37×10^{-15}	4.17×10^{-10}
280	4.02×10^{-10}	5.20×10^{-12}	2.24×10^{-26}	4.20×10^{-15}	4.07×10^{-10}
298	3.94×10^{-10}	2.78×10^{-12}	7.95×10^{-26}	4.03×10^{-15}	3.97×10^{-10}
300	3.86×10^{-10}	2.61×10^{-12}	9.18×10^{-26}	3.86×10^{-15}	3.89×10^{-10}
320	3.77×10^{-10}	1.44×10^{-12}	3.63×10^{-25}	3.71×10^{-15}	3.78×10^{-10}
340	3.68×10^{-10}	8.60×10^{-13}	1.33×10^{-24}	3.55×10^{-15}	3.69×10^{-10}
360	3.63×10^{-10}	5.48×10^{-13}	4.47×10^{-24}	3.54×10^{-15}	3.64×10^{-10}
380	3.59×10^{-10}	3.69×10^{-13}	1.37×10^{-23}	3.41×10^{-15}	3.59×10^{-10}
400	3.56×10^{-10}	2.60×10^{-13}	3.86×10^{-23}	3.37×10^{-15}	3.56×10^{-10}

Table S7 Rate coefficients of distinct SCIs reactions with Pent1a computed at different temperatures

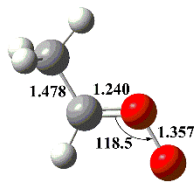
T/K	$k_{\text{CH}_2\text{OO}}(\text{R1a})$	$k_{\text{anti-CH}_3\text{CHOO}}(\text{R9})$	$k_{\text{syn-CH}_3\text{CHOO}}(\text{R10})$	$k_{(\text{CH}_3)_2\text{COO}}(\text{R11})$
273	5.0×10^{-11}	6.4×10^{-10}	2.0×10^{-13}	4.4×10^{-11}
280	4.2×10^{-11}	4.7×10^{-10}	1.9×10^{-13}	3.5×10^{-11}
298	2.7×10^{-11}	3.3×10^{-10}	1.7×10^{-13}	2.2×10^{-11}
300	2.6×10^{-11}	2.8×10^{-10}	1.7×10^{-13}	2.1×10^{-11}
320	1.7×10^{-11}	2.3×10^{-10}	1.5×10^{-13}	1.4×10^{-11}
340	1.2×10^{-11}	1.7×10^{-10}	1.4×10^{-13}	9.4×10^{-12}
360	8.5×10^{-12}	1.1×10^{-10}	1.3×10^{-13}	6.9×10^{-12}
380	6.4×10^{-12}	8.3×10^{-11}	1.2×10^{-13}	5.3×10^{-12}
400	5.0×10^{-12}	5.3×10^{-11}	1.2×10^{-13}	4.2×10^{-12}

Table S8 Predicted saturated vapour pressure (P^0) and saturated concentrations (c^0) for the adduct products of the successive reactions of SCIs with HCOOH

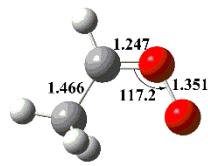
	formula	P^0 (atm)	c^0 (ug/m ³)
n CH ₂ OO + HCOOH			
n = 1	HC(O)OCH ₂ OOH	2.77×10^{-2}	1.03×10^8
n = 2	HC(O)O(CH ₂ OO) ₂ H	9.73×10^{-4}	5.42×10^6
n = 3	HC(O)O(CH ₂ OO) ₃ H	3.41×10^{-5}	2.53×10^5
n = 4	HC(O)O(CH ₂ OO) ₄ H	1.20×10^{-6}	1.11×10^4
n = 5	HC(O)O(CH ₂ OO) ₅ H	4.19×10^{-8}	4.67×10^2
n <i>anti</i> -CH ₃ CHOO + HCOOH			
n = 1	HC(O)OCH(CH ₃)OOH	1.44×10^{-2}	6.15×10^7
n = 2	HC(O)O(CH(CH ₃)OO) ₂ H	2.61×10^{-4}	1.75×10^6
n = 3	HC(O)O(CH(CH ₃)OO) ₃ H	4.73×10^{-6}	4.32×10^4
n = 4	HC(O)O(CH(CH ₃)OO) ₄ H	8.59×10^{-8}	9.92×10^2
n = 5	HC(O)O(CH(CH ₃)OO) ₅ H	1.56×10^{-9}	2.18×10^1
n <i>syn</i> -CH ₃ CHOO + HCOOH			
n = 1	HC(O)OCH(CH ₃)OOH	1.44×10^{-2}	6.15×10^7
n = 2	HC(O)O(CH(CH ₃)OO) ₂ H	2.61×10^{-4}	1.75×10^6
n = 3	HC(O)O(CH(CH ₃)OO) ₃ H	4.73×10^{-6}	4.32×10^4
n = 4	HC(O)O(CH(CH ₃)OO) ₄ H	8.59×10^{-8}	9.92×10^2
n = 5	HC(O)O(CH(CH ₃)OO) ₅ H	1.56×10^{-9}	2.18×10^1
n (CH ₃) ₂ COO + HCOOH			
n = 1	HC(O)OC(CH ₃) ₂ OOH	1.86×10^{-3}	9.02×10^6
n = 2	HC(O)O(C(CH ₃) ₂ OO) ₂ H	4.38×10^{-5}	3.43×10^5
n = 3	HC(O)O(C(CH ₃) ₂ OO) ₃ H	1.03×10^{-6}	1.11×10^4
n = 4	HC(O)O(C(CH ₃) ₂ OO) ₄ H	2.42×10^{-8}	3.35×10^2
n = 5	HC(O)O(C(CH ₃) ₂ OO) ₅ H	5.70×10^{-10}	9.57×10^0



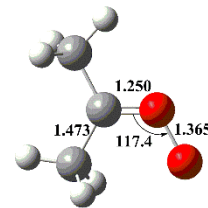
CH₂OO



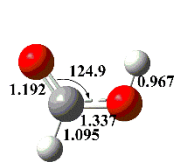
anti-CH₃CHOO



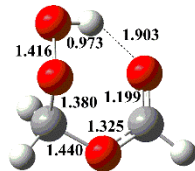
syn-CH₃CHOO



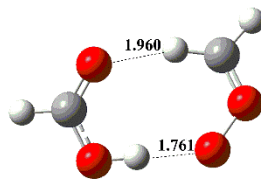
(CH₃)₂CHOO



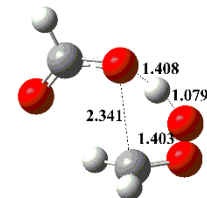
HCOOH



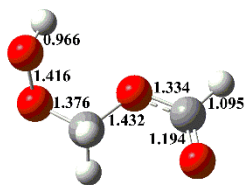
Pent1a



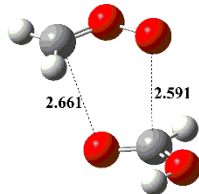
IMent2a



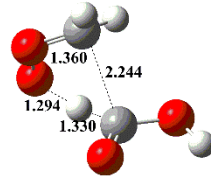
TSent2a



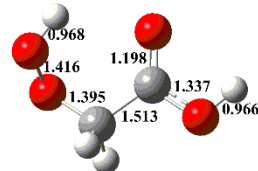
Pent2a



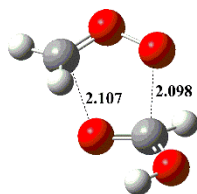
IMent3a



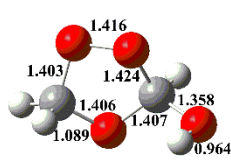
TSent3a



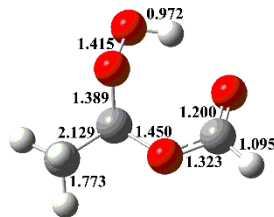
Pent3a



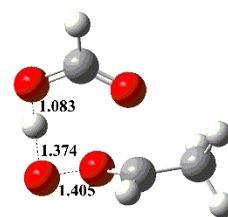
TSent4a



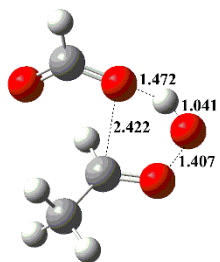
Pent4a



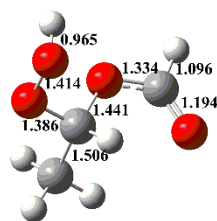
Pent1b



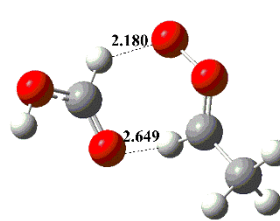
IMent2b



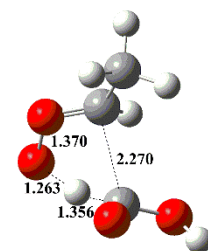
TSent2b



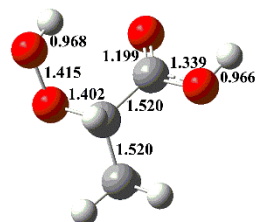
Pent2b



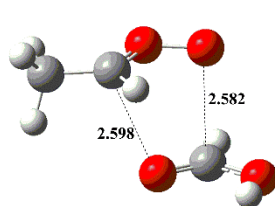
IMent3b



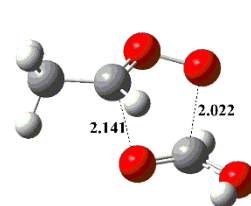
TSent3b



Pent3b



IMent4b



TSent4b

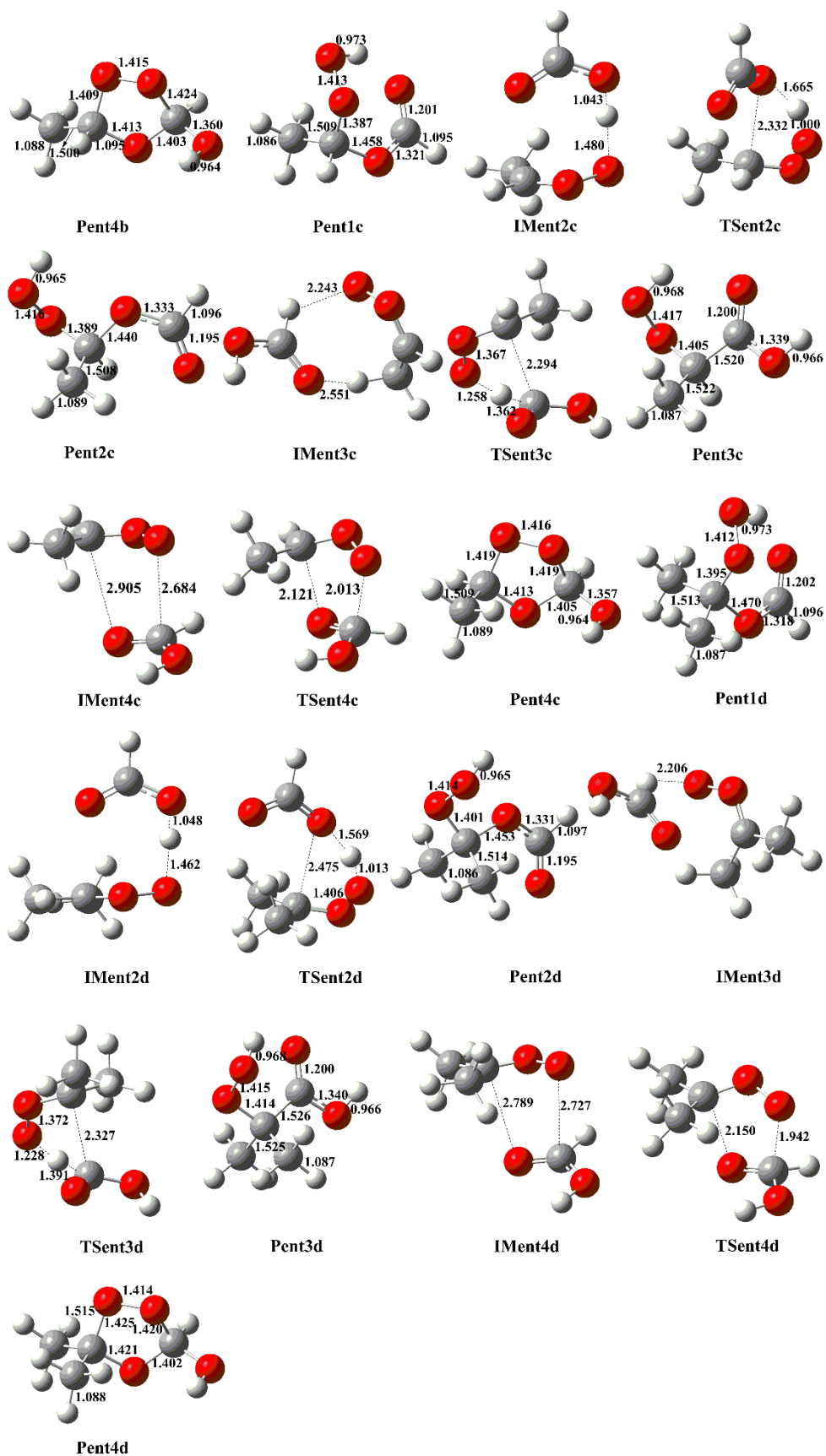


Figure S1. The geometries of all the stationary points for distinct SCIs reactions with formic acid optimized at the M06-2X/6-311+G(2df,2p) level of theory

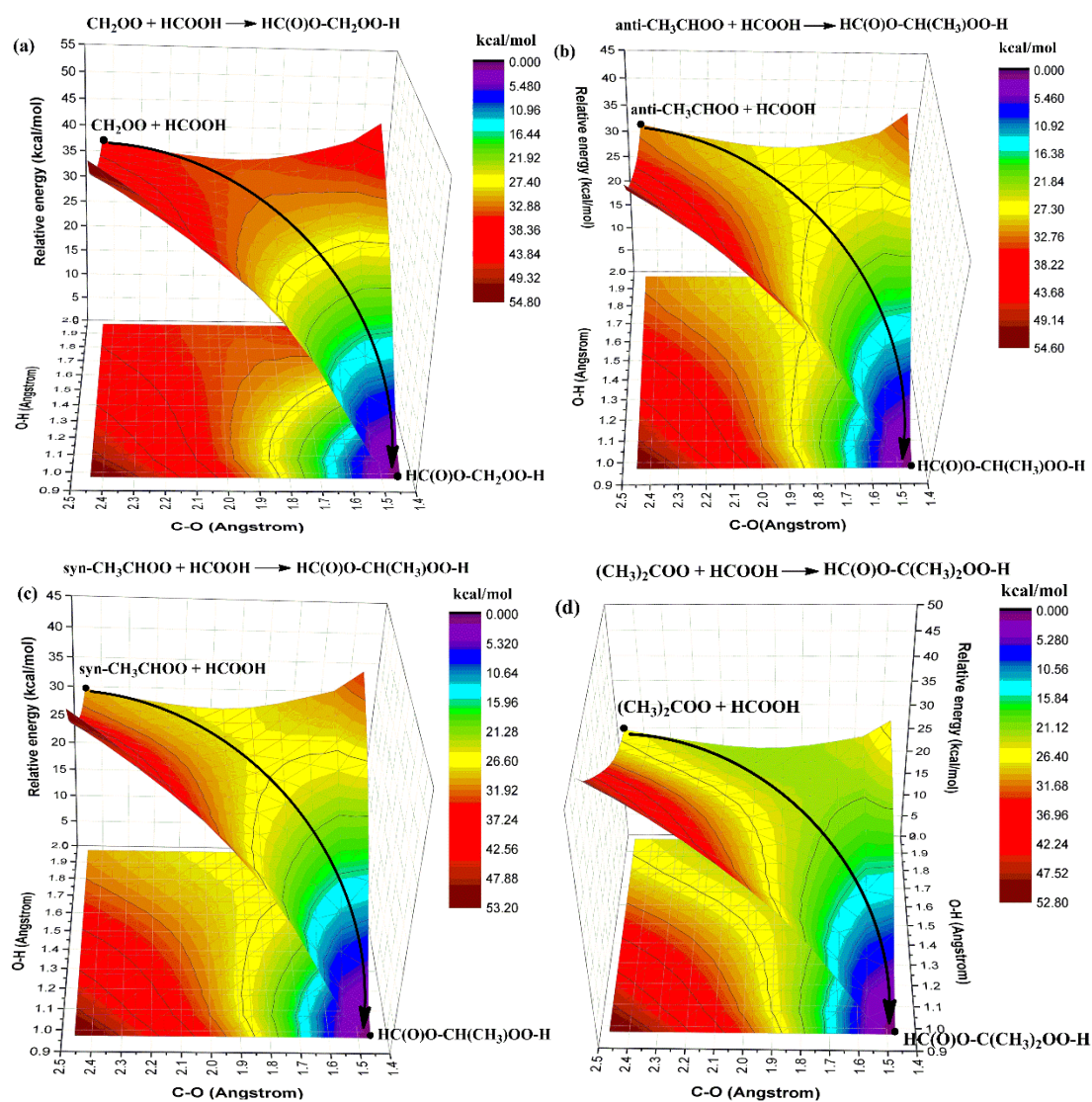


Figure S2. Electronic potential energy along the O-H and C-O distance (angstroms) calculated by the M06-2X/6-311+G(2df,2p) method for the 1,4-insertion reactions $\text{CH}_2\text{OO} + \text{HCOOH}$ (a), *anti*- $\text{CH}_3\text{CHO} + \text{HCOOH}$ (b), *syn*- $\text{CH}_3\text{CHO} + \text{HCOOH}$ (c) and $(\text{CH}_3)_2\text{COO} + \text{HCOOH}$ (d) (the black solid line represents the minimum potential-energy path (MEP))

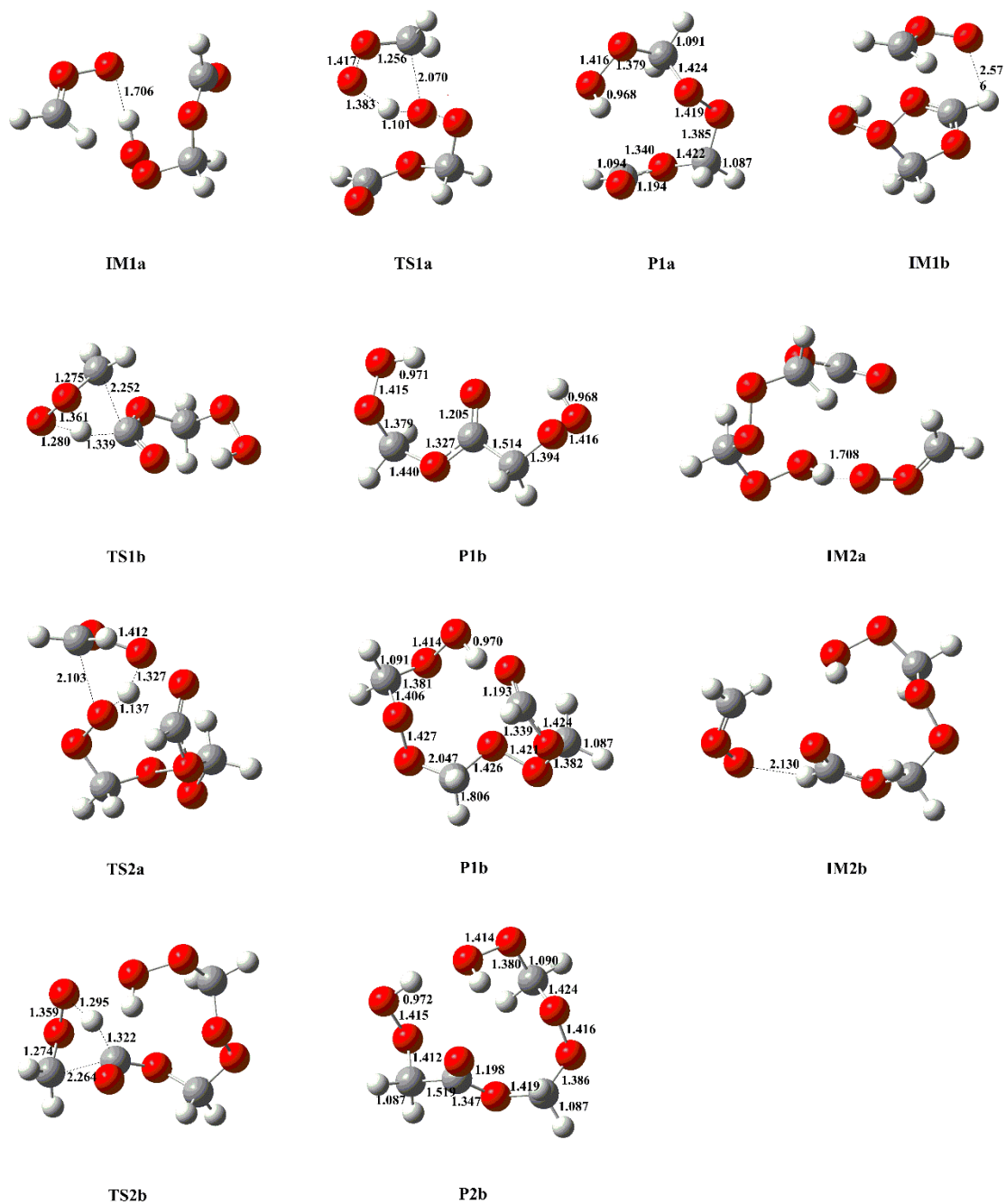


Figure S3. The geometries of all the stationary points for $2\text{CH}_2\text{OO} + \text{Pent1a}$ reaction optimized at the M06-2X/6-311+G(2df,2p) level of theory

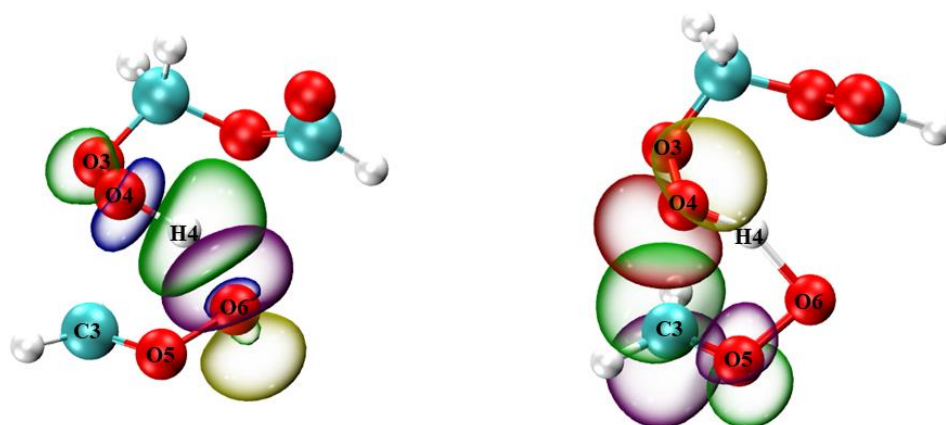


Figure S4. Natural bond orbital (NBO) analysis of the donor-acceptor orbitals involved in the TS1a

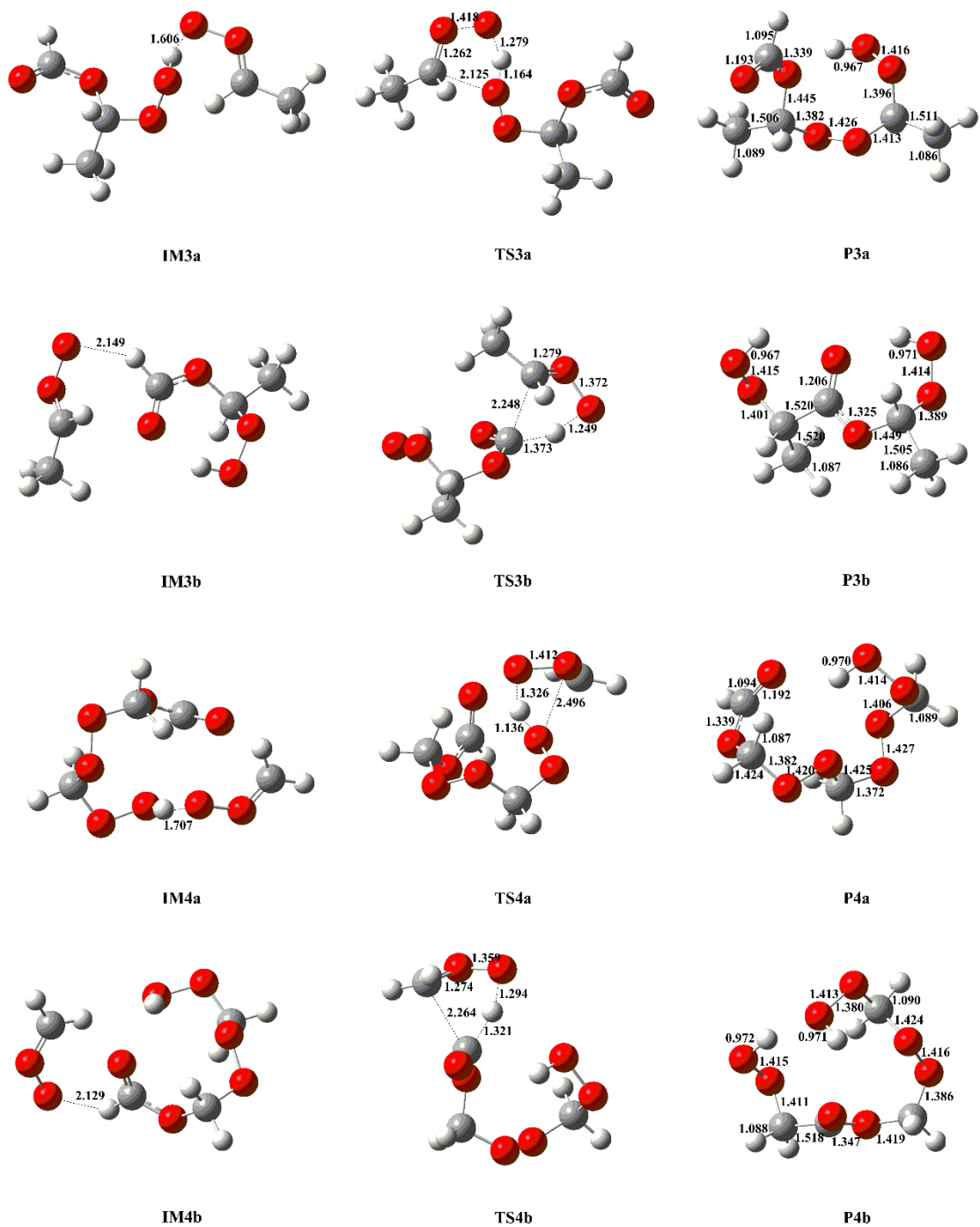


Figure S5. The geometries of all the stationary points for $2anti\text{-CH}_3\text{CHOO} + \text{Pent1b}$ reaction optimized at the M06-2X/6-311+G(2df,2p) level of theory

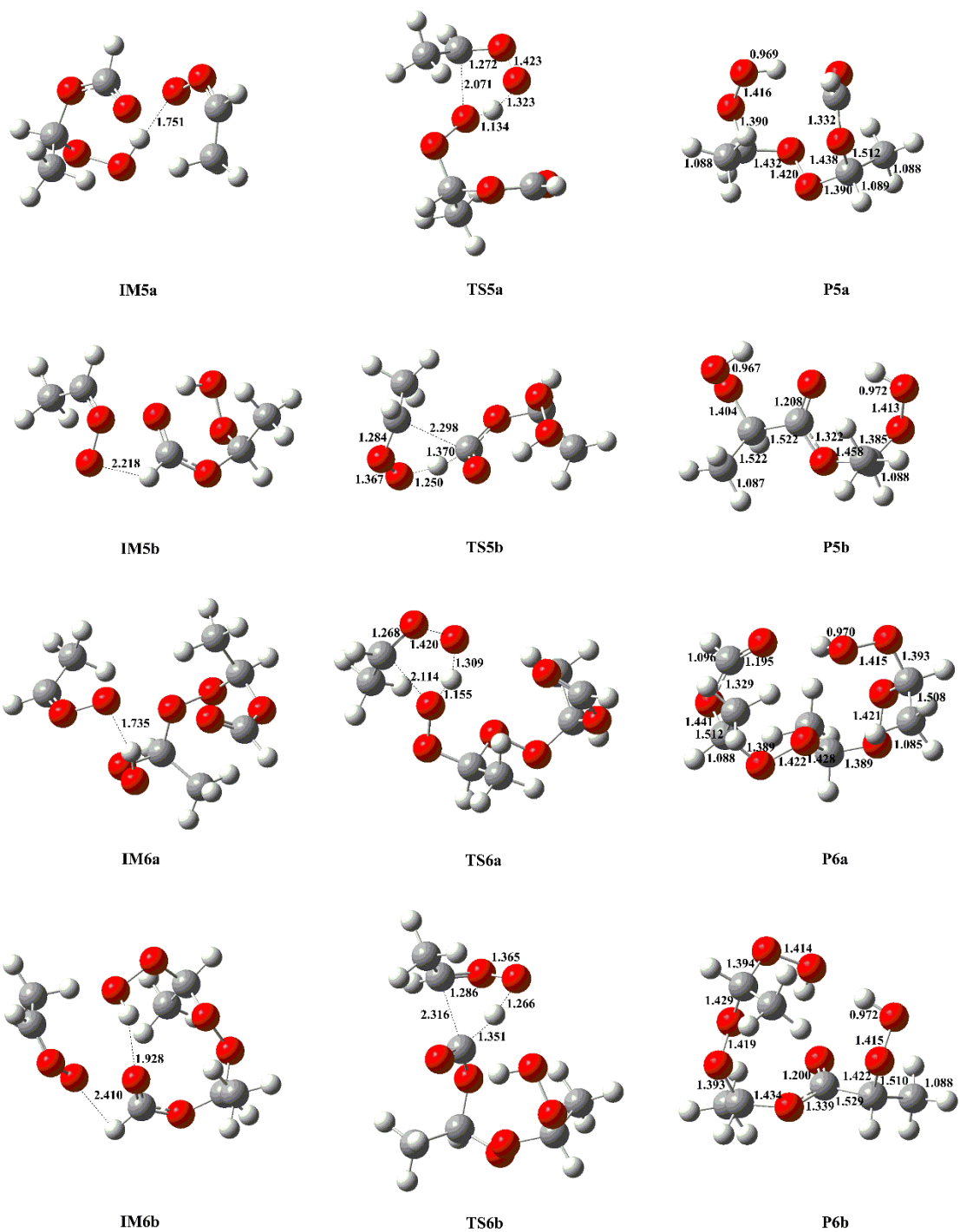


Figure S6. The geometries of all the stationary points for 2*syn*-CH₃CHOO + Pent1c reaction optimized at the M06-2X/6-311+G(2df,2p) level of theory

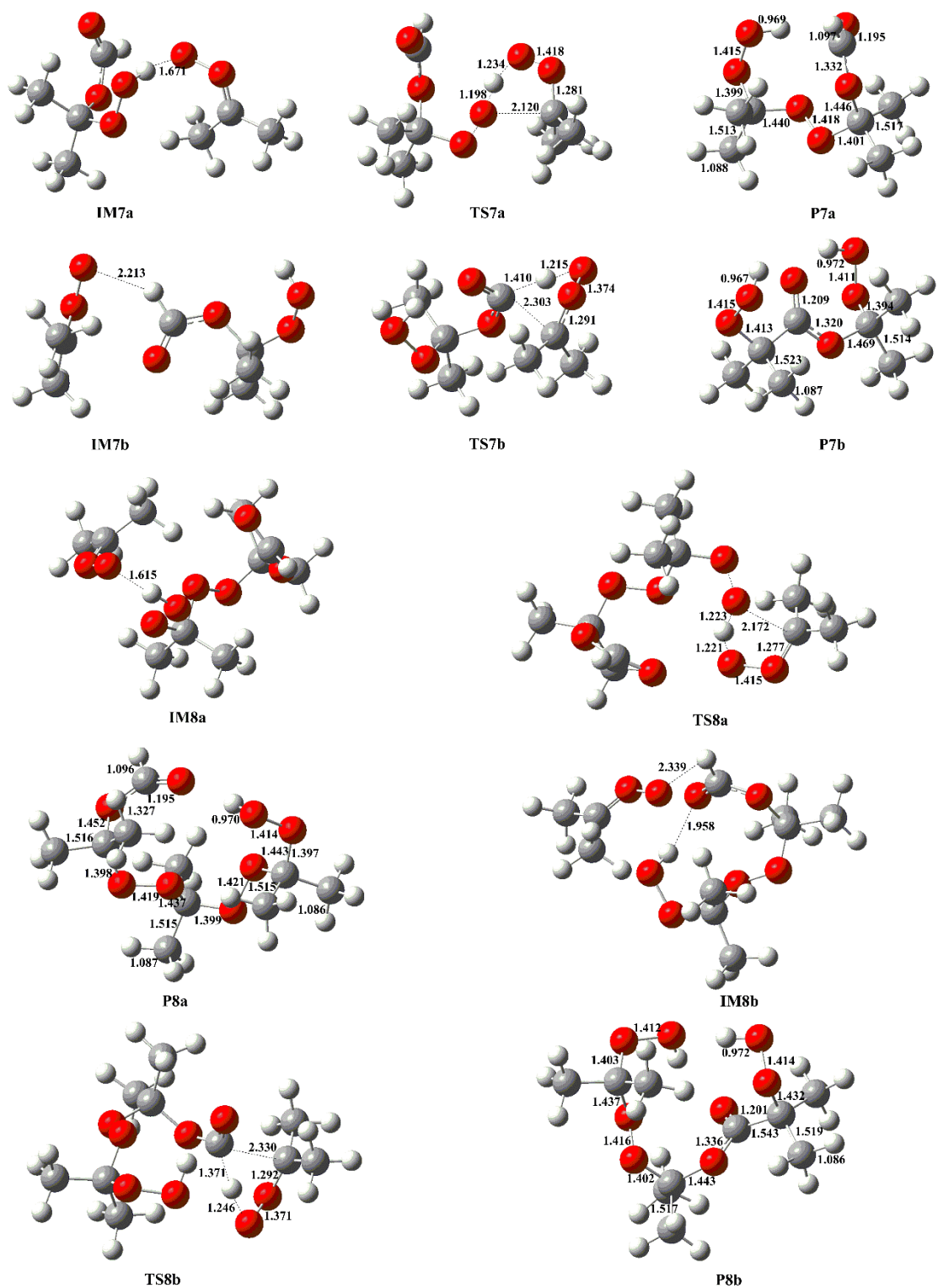


Figure S7. The geometries of all the stationary points for 2(CH₃)₂COO + Pent1d reaction optimized at the M06-2X/6-311+G(2df,2p) level of theory

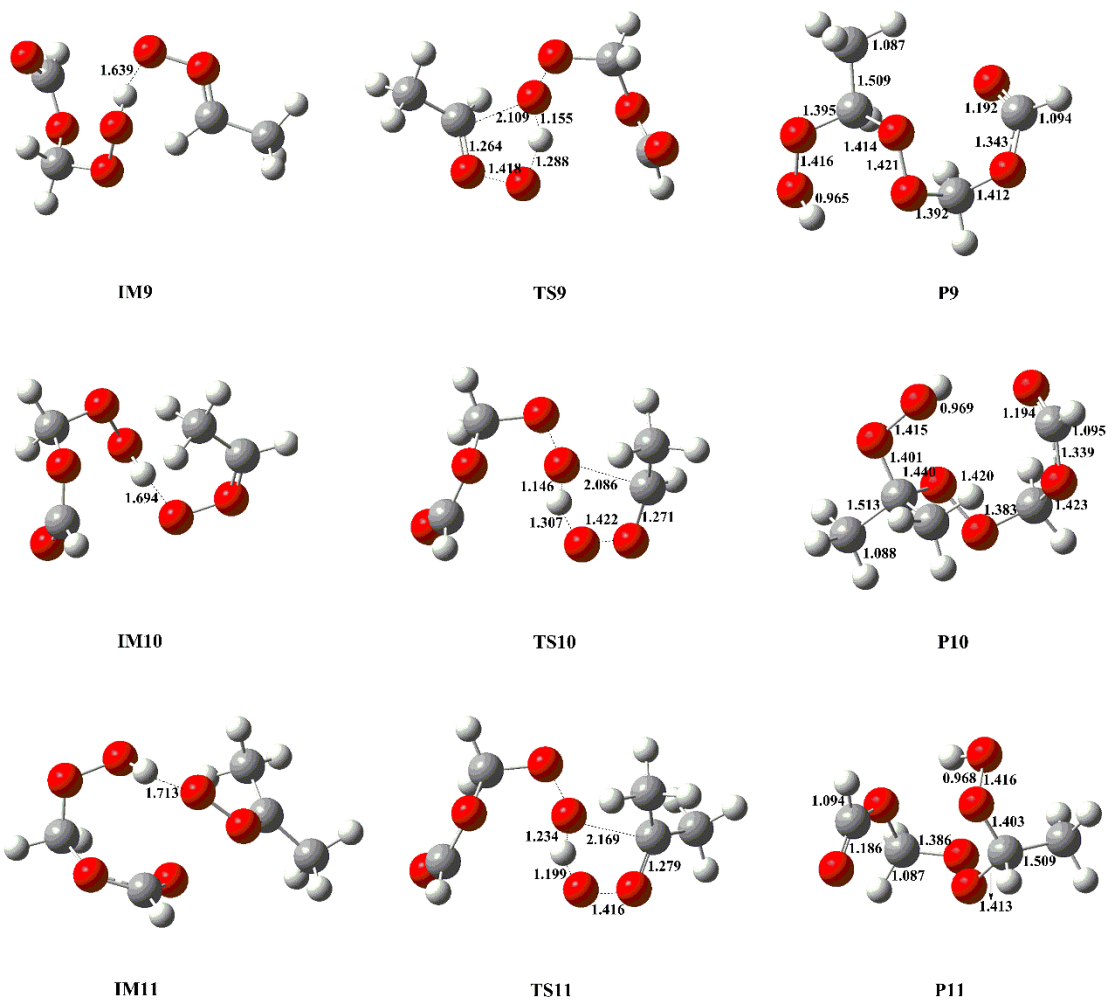


Figure S8. The geometries of all the stationary points for distinct SCIs reactions with Pent1a optimized at the M06-2X/6-311+G(2df,2p) level of theory

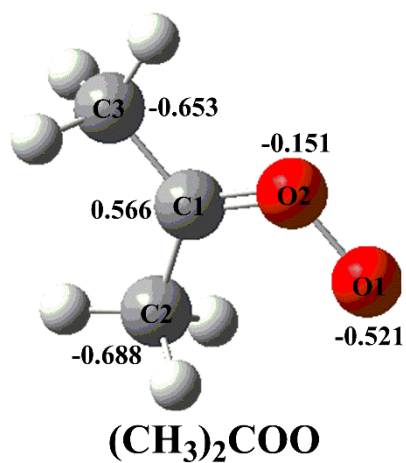
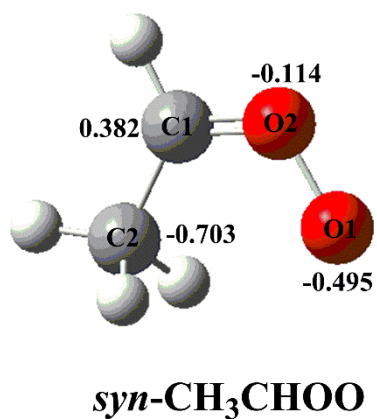
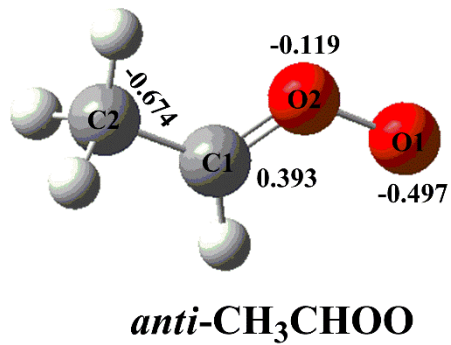
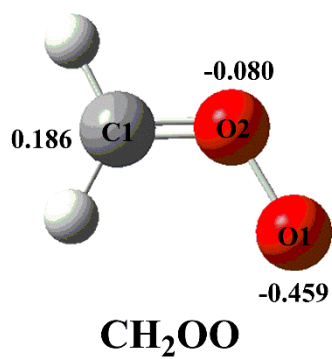


Figure S9 The NPA charges of different atoms in the distinct SCIs computed at the M06-2X/6-311+g(2df,2p) level of theory

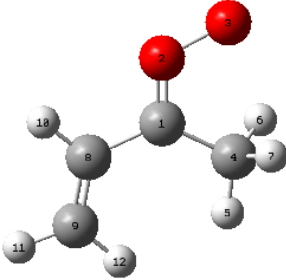
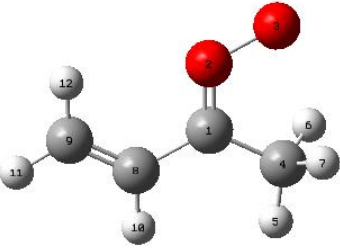
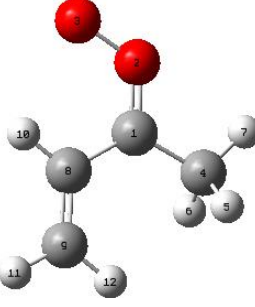
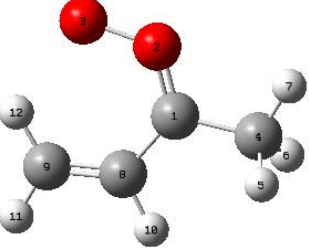
	trans	cis
syn	 0.00	 1.42
anti	 2.43	 2.69

Figure S10. The optimized geometries and relative energies ($\text{kcal}\cdot\text{mol}^{-1}$) computed for the four conformers of MVK-oxide. Geometries are optimized at the M06-2X/6-311+g(2df,2p) level of theory. Single point energies are calculated at the CCSD(T)/6-311+g(2df,2p) level of theory